Introduction and recovery of point defects in electron-irradiated ZnO

F. Tuomisto* and K. Saarinen
Laboratory of Physics, Helsinki University of Technology, P.O. Box 1100, 02015 TKK, Finland

D. C. Look
Semiconductor Research Center, Wright State University, Dayton, Ohio 45435, USA
and Materials and Manufacturing Directorate, Air Force Research Laboratory, Wright-Patterson AFB, Ohio 45433, USA

G. C. Farlow
Physics Department, Wright State University, Dayton, Ohio 45435, USA
(Received 6 April 2005; revised manuscript received 13 June 2005; published 3 August 2005)

We have used positron annihilation spectroscopy to study the introduction and recovery of point defects in electron-irradiated *n*-type ZnO. The irradiation ($E_{el}=2$ MeV, fluence 6×10^{17}cm^{-2}) was performed at room temperature, and isochronal annealings were performed from 300 to 600 K. In addition, monochromatic illumination of the samples during low-temperature positron measurements was used in identification of the defects. We distinguish two kinds of vacancy defects: the Zn and O vacancies, which are either isolated or belong to defect complexes. In addition, we observe negative-ion-type defects, which are attributed to O interstitials or O antisites. The Zn vacancies and negative ions act as compensating centers and are introduced at a concentration $[V_{Zn}]\simeq c_{ion}\simeq 2\times10^{16}$cm^{-3}. The O vacancies are introduced at a 10-times-larger concentration $[V_O]\simeq 3\times10^{17}$cm^{-3} and are suggested to be isolated. The O vacancies are observed as neutral at low temperatures, and an ionization energy of 100 meV could be fitted with the help of temperature-dependent Hall data, thus indicating their deep donor character. The irradiation-induced defects fully recover after the annealing at 600 K, in good agreement with electrical measurements. The Zn vacancies recover in two separate stages, indicating that the Zn vacancies are parts of two different defect complexes. The O vacancies anneal simultaneously with the Zn vacancies at the later stage, with an activation energy of $E^m_{V,O}=1.8\pm0.1$ eV. The negative ions anneal out between the two annealing stages of the vacancies.

DOI: 10.1103/PhysRevB.72.085206 PACS number(s): 61.72.Ji, 61.82.Fk, 78.20.Ek, 78.70.Bj

I. INTRODUCTION

Interest in zinc oxide (ZnO) has grown during the recent years due to progress in crystal growth[1] and its unique optical and electrical properties. ZnO has a direct band gap of about 3.4 eV at 2 K, similarly to gallium nitride (GaN), for which it can be thought of as an alternative for use in optoelectronic devices. The recent reports on successful *p*-type doping of ZnO (Refs. 2–4) have led to even higher expectations about the material's potential applications in electronics. In addition, when doped with manganese, ZnO has been reported to exhibit ferromagnetic behavior above room temperature,[5] making it a prospective material for spintronics applications.

Point defects have an important effect on the electronic and optoelectronic properties of semiconductor materials. Both their identification and quantification are necessary in order to understand the microscopic processes leading to the specific properties. Point defects are created in semiconductors during growth, where their formation is governed by thermodynamics and growth kinetics. They can be introduced in concentrations much larger than those given by the thermodynamic equilibrium by means of irradiation of the material—e.g., by electrons. The study of the formation of point defects under these nonequilibrium conditions gives information on the basic physical properties of the semiconductor material.

Defects introduced by electron and neutron irradiation in ZnO have been studied by electron paramagnetic resonance (EPR) in the past[6–11] and also quite recently.[12,13] Signals from both Zn and O interstitials[12] and from Zn vacancies[6–9] have been observed only at temperatures well below the room temperature—i.e., at 4–90 K. The disparition of the signals has been reported to occur at several stages between 110 K and 280 K. Only the O vacancies have been observed with EPR at room temperature.[8,10,11,13] The photoluminescence spectrum of ZnO typically exhibits a green luminescence (GL) band similar to the yellow luminescence in GaN.[14] Both the Zn (Refs. 14,15) and O (Refs. 16–18) vacancies have been proposed to be the defect responsible for this GL band. However, the conclusive identification is still lacking.

Both the optical and electrical properties of ZnO are much more resistant than those of GaN to deterioration caused by room-temperature electron and proton irradiation,[19–21] which makes it potentially useful for applications in high-irradiation environments. The apparent radiation hardness remains when the irradiation is performed at a low temperature of 130 K,[22] indicating that the primary irradiation-induced compensating defects are mobile already at those temperatures. The microscopic origin of the radiation hardness of ZnO is not, however, well understood.

In this work we investigate the introduction and thermal recovery of the point defects created in ZnO by room-temperature irradiation with 2-MeV electrons. To do this we apply positron annihilation spectroscopy, which is sensitive to defects with open volume. Positrons get trapped at va-

cancy defects, which changes their annihilation characteristics. The positron lifetime reflects the open volume of the defect. On the other hand, the Doppler broadening of the 511-keV annihilation radiation gives information about the electron momentum distribution at the annihilation site and is sensitive to the atomic environment of the vacancy. The combination of these techniques can thus be used to identify both the open volume and the sublattice of the defect in compound semiconductors.

We observe three kinds of point defects produced by the electron irradiation ($E_{el}=2$ MeV, fluence 6×10^{17} cm^{-2}): the Zn and O vacancies or complexes involving the vacancies and negative-ion-type defects, which are attributed to O interstitials or O antisites. The Zn vacancies and negative-ion-type defects act as compensating centers and are introduced at a concentration $[V_{Zn}]\simeq c_{st}\simeq 2\times10^{16}$ cm^{-3}. The O vacancies are introduced at a 10-times-larger concentration $[V_O]\simeq 3\times10^{17}$ cm^{-3}. The O vacancies are observed as neutral at low temperatures, and an ionization energy of 100 meV could be fitted with the help of temperature-dependent Hall data, thus indicating their deep donor character. By shining monochromatic light on the samples during the positron annihilation measurements at low temperature, we find that both the Zn vacancies and the negative-ion-type defects have ionization levels close to 2.3 eV. Thus both defects are possibly involved in the green luminescence exhibited by ZnO.[14,17] The irradiation-induced defects fully recover after the annealing at 600 K, in good agreement with electrical measurements.[19] The Zn vacancies anneal out of the material in two stages with fitted activation energies $E_{A1}^{V,Zn}\simeq 1.3$ eV and $E_{A2}^{V,Zn}\simeq 1.8$ eV, indicating that the Zn vacancies are parts of two different defect complexes. The O vacancies anneal simultaneously with the Zn vacancies at the later stage with fitted activation energy $E_A^{V,O}\simeq 1.8$ eV. The O vacancies are suggested to be isolated, and hence the activation energy can be interpreted as the migration barrier of the O vacancy. The negative-ion-type defects anneal out between the two annealing stages of the Zn and O vacancies.

II. METHOD

A. Experimental details

The positron lifetime experiments were performed in nominally undoped single-crystal ZnO samples grown by the seeded vapor phase technique. Two samples were irradiated with 2-MeV electrons to a fluence 6×10^{17} cm^{-3}. The irradiations were performed with a current density of 2 A/cm^2 at room temperature, in a vacuum of $1–5\times10^{-6}$ torr. Both the as-grown and irradiated samples were *n* type (in as-grown $N_e\simeq 1\times10^{17}$ cm^{-3} and in irradiated $N_e\simeq 3\times10^{15}$ cm^{-3}), most likely due to residual H and Al. After irradiation, the samples were mounted to a closed-cycle liquid helium cryostat for positron measurements as a function of isochronal annealing between 300 and 600 K. The 30-min annealings were performed *in situ* in the positron measurement cryostat in a vacuum of 10^{-6} mbar. The positron lifetime measurements were performed at 20, 80, 150, and 300 K.

The positron measurement cryostat was equipped with a possibility to shine monochromatic light on the samples during lifetime measurements. These measurements were performed under monochromatic illumination with sub-band-gap ($h\nu=0.7–3.1$ eV) light. The photon flux was kept constant during each measurement, but at high photon energies only a somewhat lower flux was obtained due to limitations in the intensity of the light source (halogen lamp). Photon fluxes between 10^{14} and 10^{15} cm^{-2} s^{-1} were used. Additionally, two 540-nm green lasers were used to produce a photon flux 6×10^{15} cm^{-2} s^{-1} at photon energy $h\nu=2.3$ eV. All the measurements of the photoexcitation of the defects were performed at 20 K.

The positron lifetimes were measured with a conventional fast-fast coincidence spectrometer with a time resolution of 250 ps.[23] Two identical sample pieces were sandwiched with a 20-μCi positron source (^{22}Na deposited on 1.5-μm Al foil). Typically 2.5×10^6 and 5×10^6 annihilation events were collected in each positron lifetime spectrum in the annealing experiments and in the photoexcitation experiments, respectively. The lifetime spectrum $n(t)=\Sigma_i I_i\exp(-t/\tau_i)$ was analyzed as the sum of exponential decay components convoluted with the Gaussian resolution function of the spectrometer, after subtracting the constant background and annihilations in the source material (200 ps, 2.0%; 400 ps, 5.8%; 1500 ps, 0.06%). The positron in state *i* annihilates with a lifetime τ_i and an intensity I_i. The state in question can be the delocalized state in the lattice or the localized state at a vacancy defect. The increase of the average lifetime $\tau_{ave}=\Sigma_i I_i\tau_i$ above the bulk lattice lifetime τ_B shows that vacancy defects are present in the material. This parameter is insensitive to the decomposition procedure, and even as small a change as 1 ps in its value can be reliably measured.

In the case of one type of vacancy defect with specific lifetime τ_V, the decomposition of the lifetime spectrum into two components τ_1 and τ_2 is straightforward to interpret. The second lifetime component $\tau_2=\tau_V$ gives directly the vacancy-specific lifetime and the first lifetime component is $\tau_1=(\tau_B^{-1}+\kappa_V)^{-1}<\tau_B$, where τ_B is the positron lifetime in the delocalized state in the lattice and κ_V the positron trapping rate into the vacancy defects.

The Doppler broadening of the annihilation radiation was measured simultaneously with the positron lifetime using a Ge detector with an energy resolution of 1.3 keV. The conventional valence (*S*, low momenta: $|p_z|<3\times10^{-3}m_0c$) and core (*W*, high momenta: $10\times10^{-3}m_0c<|p_z|<30\times10^{-3}m_0c$) annihilation parameters were determined from the measured data after background subtraction as the fractions of annihilations in the corresponding momentum ranges. The parameters are presented here as relative to the parameters specific to the annihilation from the delocalized state in the perfect ZnO lattice.

B. Data analysis

1. Positron trapping at defects

The temperature dependence of the positron annihilation parameters (τ_{ave}, *S*, and *W*) is analyzed with the model of trapping and escape rates of positrons, explained in detail in

earlier works.[23–26] In this model, the trapping coefficient μ_V to a neutral vacancy is independent of temperature and to a negatively charged vacancy it varies as $T^{-0.5}$. The trapping rate of positrons into the vacancies (concentration c_V) is $\kappa_V = \mu_V c_V$. Positrons can get trapped also at hydrogenlike Rydberg states surrounding negative-ion-type defects (shallow traps for positrons). The positron trapping rate at the Rydberg state μ_R varies also as $T^{-0.5}$, which is the result predicted by theory for the transition from a free state to a bound state in a Coulomb potential.[26] The thermal escape rate from the Rydberg state can be written as

$$\delta_{\mathrm{st}} = \mu_{\mathrm{R}} \left(\frac{m_+ k_B T}{2\pi\hbar^2} \right)^{3/2} \exp(-E_{b,\mathrm{st}}/k_B T), \tag{1}$$

where μ_R is the positron trapping coefficient to the lowest hydrogenlike Rydberg state, $E_{b,\mathrm{st}}$ is the positron binding energy of the lowest Rydberg state (typically <0.1 eV), and $m_+ \simeq m_0$ is the effective mass of the positron. In principle, positrons can also escape from the Rydberg states around negatively charged vacancies, but we assume that the transition from the Rydberg state to the ground state in the vacancy is fast enough so that this effect can be neglected. This is supported by the results obtained previously in both ZnO (Ref. 21) and GaN (Ref. 27). An effective trapping rate of the shallow traps can thus be defined as

$$\kappa_{\mathrm{st}}^{\mathrm{eff}} = \frac{\kappa_{\mathrm{st}}}{1 + \delta_{\mathrm{st}}/\lambda_{\mathrm{st}}}, \tag{2}$$

where $\lambda_{\mathrm{st}} \simeq \lambda_B$ is the annihilation rate of positrons trapped at the Rydberg state, which coincides with the annihilation rate λ_B from the delocalized state in the bulk lattice, and $\kappa_{\mathrm{st}} = \mu_R c_{\mathrm{st}}$ is directly related to the concentration of the negative ions.

The temperature dependence of the positron data can also arise from a change in the charge state of the positron trapping defect (vacancy or negative ion) due to the dependence of the Fermi level E_F on temperature. Then a vacancy that is neutral (as is expected for, e.g., the O vacancy) at low temperatures can be ionized and become positive and thus repulsive to positrons when the temperature is raised. Then the trapping rate can change even if the trapping coefficient itself is constant as a function of temperature. The ratio of neutral to all (neutral and positive) vacancies can be written as

$$\frac{[V^0]}{[V^0]+[V^+]} = \left[1 + g^{-1} \exp\left(\frac{E_i - E_F(T)}{k_B T} \right) \right]^{-1}, \tag{3}$$

where E_i is the ionization energy of the neutral vacancy and g the ratio of internal degeneracies of the two charge states.

In addition, the effective trapping of positrons into neutral defects can depend on temperature if the binding energy is low enough. A typical positron binding energy to a vacancy is ~ 1 eV, and thus in the above equations the escape rate of the positrons from the ground state in the vacancy is assumed to be very low compared to the positron lifetime. However, in the case of the N vacancy in GaN or the O vacancy in ZnO, where the missing atom is very small compared to the neighboring atoms, the binding energy can be of the same order of magnitude as the Rydberg state of a negative ion. In such a case, the temperature dependence of the thermal detrapping causes a temperature dependence in the effective trapping rate to the neutral vacancy.

2. Kinetic trapping model

The decomposition of the lifetime spectra into several lifetime components gives the possibility to determine experimentally the fractions of positrons annihilating in various states. The average lifetime can be written as[23]

$$\tau_{\mathrm{ave}} = \eta_B \tau_B + \sum_j \eta_{D,j} \tau_{D,j}, \tag{4}$$

where η_B and τ_B are the annihilation fraction and positron lifetime in the free state in the lattice, and $\eta_{D,j}$ and $\tau_{D,j}$ are the corresponding values in bound states at the defect D_j. The annihilation fractions are related to the trapping rates through

$$\eta_B = \frac{\lambda_B}{\lambda_B + \sum_j \kappa_{D,j}^{\mathrm{eff}}}, \quad \eta_{D,j} = \frac{\kappa_{D,j}^{\mathrm{eff}}}{\lambda_B + \sum_{j'} \kappa_{D,j'}^{\mathrm{eff}}}. \tag{5}$$

Equation (4) can be fitted to the τ_{ave} vs T data, using the trapping rates and the possible binding energies to the Rydberg states as fitting parameters. Another possibility is to write the trapping rate $\kappa_{D,j}^{\mathrm{eff}}$ to a defect D_j as a function of the experimental parameters:

$$\kappa_{D,j}^{\mathrm{eff}} = \lambda_B \frac{\tau_{\mathrm{ave}} - \tau_B}{\tau_{D,j} - \tau_{\mathrm{ave}}} - \sum_{j' \neq j} \kappa_{D,j'}^{\mathrm{eff}} \frac{\tau_{D,j'} - \tau_{\mathrm{ave}}}{\tau_{D,j} - \tau_{\mathrm{ave}}}. \tag{6}$$

In the case of only one type of defect, the sum in Eq. (6) vanishes and the trapping rate can be calculated directly from the experimental values of τ_{ave}, $\tau_{D,j}$, and τ_B. If several defect types are present, the trapping rates to the other defects need to be known.

III. IDENTIFICATION OF THE DEFECTS

A. Positron data

The results of the positron lifetime and Doppler broadening measurements in both the as-grown and irradiated ZnO samples are presented as a function of measurement temperature in Fig. 1. The increase of the average positron lifetime τ_{ave} with decreasing temperature is a clear indication of the presence of negatively charged vacancy defects. In the as-grown material, the monotonous behavior of the lifetime below 300 K indicates that these vacancy defects are the dominant negatively charged defect. On the other hand, in the electron-irradiated samples the decrease of the positron lifetime with decreasing temperature is typical of negative-ion-type defects that compete in trapping of positrons with the negative vacancies. This is observed also as the increase of the first lifetime component τ_1, where the increased trapping in the negative-ion-type defects brings the component closer to the bulk lifetime. The Doppler broadening parameters S and W behave as a function of temperature similarly to the positron lifetime.

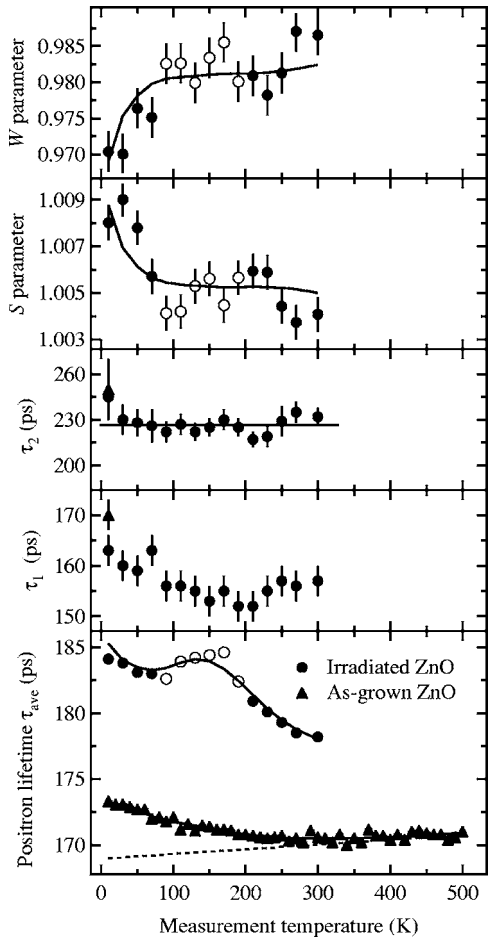

FIG. 1. The positron lifetime and Doppler broadening parameters of the as-grown and irradiated samples plotted as a function of measurement temperature. The solid curves represent the parameters obtained by fitting the temperature-dependent trapping model to the data. The dashed line shows the fitted bulk lifetime, where the temperature dependence is due to the thermal expansion of the lattice. The circles are drawn as open in the temperature range 90–190 K, where the effect of the oxygen vacancies is most visible.

A higher lifetime component of $\tau_V=\tau_2=230\pm10$ ps could be extracted from the exponential lifetime spectra below 300 K, while the data measured in the as-grown ZnO sample above 300 K were purely one-componential. The higher lifetime component is constant as a function of temperature, which implies that it represents positrons annihilating in one bound state. In our previous study, we have identified this higher lifetime component as that specific to the Zn vacancy and the lifetime $\tau_B=170$ ps to the annihilation from the delocalized state in the ZnO lattice at 300 K.[21] Also the Doppler broadening parameters ($S_D=1.039$ and $W_D=0.87$) specific to the Zn vacancy were determined in that work. By comparing the positron results to temperature-dependent Hall measurements, the Zn vacancy in the double-negative-charge state was identified as the dominant compensating defect (concentration $[V_{\mathrm{Zn}}]\simeq2\times10^{15}\mathrm{cm}^{-3}$) in as-grown ZnO and co dominant together with the so-far-unidentified negative-ion-type defect [prominent candidates are the O interstitial and O antisite, which, according to theory, are negative in *n*-type ZnO (Ref. 15)] in the irradiated material, where the concentrations of both defects were obtained as $[V_{\mathrm{Zn}}]\simeq c_{\mathrm{st}}\simeq2\times10^{16}\mathrm{cm}^{-3}$. The identification was based on both positron lifetime and Doppler broadening coincidence measurements together with comparison to theoretical positron calculations. In addition, the Zn vacancies were the main defect observed by positron annihilation spectroscopy.

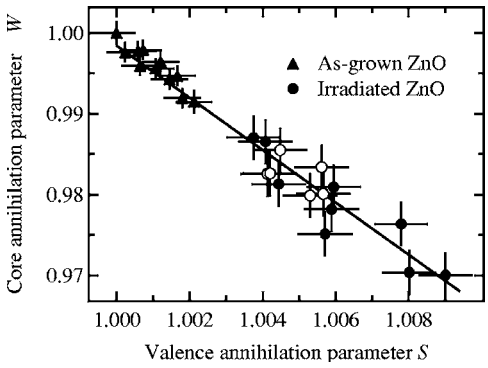

FIG. 2. The *W* parameter plotted as a function of the *S* parameter. The dependence is linear, indicating the presence of one type of vacancy defects. The open circles were measured at $T=90$–190 K. The solid line is fitted to the data.

The Doppler broadening parameters *S* and *W* fall on a line when plotted against each other with temperature as the running parameter (Fig. 2), which typically indicates the presence of only two distinguishable positron states (bulk and vacancy). The negative-ion-type defects do not cause deviations from the straight line, since the annihilation parameters of positrons trapped at these shallow traps coincide with the bulk parameters.

However, as can be seen in Fig. 3, the points measured at 90–190 K in the irradiated samples fall off the straight line determined by the annihilations in the bulk lattice and the Zn vacancy. This implies that a third positron state can be distinguished in the lifetime versus Doppler parameter data although the Doppler data itself are linear. In order to cause a deviation from the straight line, the localization to this defect needs to be strong, implying that the defect has a distinguishable open volume. The open volume of this defect cannot be very large, since, as pointed out above, the independence of temperature of the higher lifetime component τ_2 shows no evidence of the mixing of several lifetime components. Hence, the lifetime specific to this defect needs to be sufficiently far from τ_2 (and closer to τ_1), below 200 ps. In addition, in order to produce the deviation observed in Fig. 3, the defect-specific lifetime needs to be above τ_{ave} over the whole temperature range—i.e., above 185 ps.

One additional aspect of the third type of defects is evident from the τ_{ave} vs *T* data. The fraction of positrons annihilating as trapped at this defect is vanishing at room temperature and clearly smaller than the annihilation fractions to the Zn vacancies and negative-ion-type defects below 90 K, but larger at the intermediate temperature 90–190 K. This implies that enhancement of positron trapping with decreasing temperature is larger in this defect at temperatures 190–300 K, but saturates around 150 K, where the Zn vacancies and negative-ion-type defects become more important. This

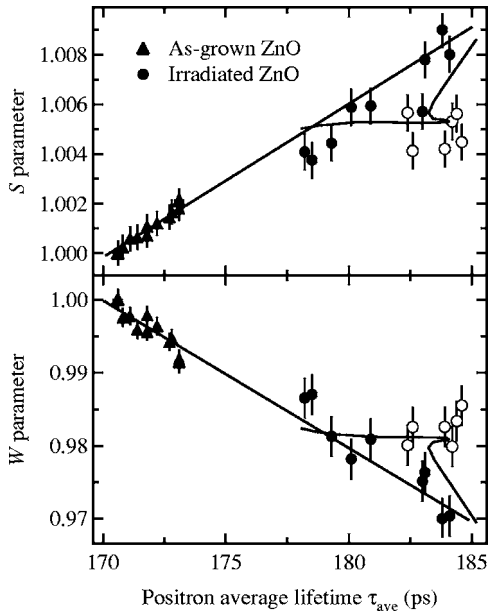

FIG. 3. The S and W parameters plotted as a function of τ_{ave}. The parameters depend linearly on each other in the temperature range where the low-binding-energy positron traps do not contribute significantly. The open circles were measured at $T=90$–190 K. The solid lines connect the parameters of the bulk lattice to those (not shown) of the Zn vacancy. The solid curves are obtained from the fits to the S vs T, W vs T, and τ_{ave} vs T data.

indicates that the third type of defect is neutral and the temperature dependence of the positron trapping observed at high temperatures is due to either thermal escape from the defect or a change in the charge state of the defect. Based on these considerations and especially the lifetime value of 190–200 ps, a prominent candidate for this defect is the O vacancy, which has a donor nature and would naturally have a smaller open volume than the Zn vacancy.

In summary, the positron data show the presence of three different defects: the negatively charged Zn vacancy ($\tau_{V,\mathrm{Zn}}=230\pm10$ ps), the neutral (at low temperatures) O vacancy ($\tau_{V,\mathrm{O}}=190$–200 ps), and the negative-ion-type defect, tentatively identified as the O interstitial or O antisite.

B. Analysis

The temperature-dependent trapping model can be used to estimate the trapping rates to the different defects from the τ_{ave} vs T data in Fig. 1 using the defect-specific positron lifetimes $\tau_{V,\mathrm{Zn}}=230$ ps, $\tau_{V,\mathrm{O}}=195$ ps, and $\tau_{\mathrm{st}}=170$ ps for the Zn vacancies, O vacancies, and negative-ion-type defects, respectively. A good first approximation can be obtained by using Eq. (6) and assuming that at 300 K only the Zn vacancies trap positrons, giving

$$\kappa_{V,\mathrm{Zn}}=\lambda_B\frac{\tau_{\mathrm{ave}}-\tau_B}{\tau_{V,\mathrm{Zn}}-\tau_{\mathrm{ave}}}\simeq 0.2\lambda_B\simeq 1.2\times10^{9}\mathrm{s}^{-1}. \quad (7)$$

At 30 K the positron data are dominated by the annihilations in the Zn vacancies and the negative-ion-type defects due to the fast increase in the trapping coefficient at low temperatures, where also S and W vs τ_{ave} are linear; thus, the trapping rate to the negative-ion-type defects (at 30 K) can be estimated as

$$\kappa_{\mathrm{st}}=\kappa_{V,\mathrm{Zn}}\frac{\tau_{V,\mathrm{Zn}}-\tau_{\mathrm{ave}}}{\tau_{\mathrm{ave}}-\tau_B}-\lambda_B\simeq 0.5\lambda_B. \quad (8)$$

Here we have used the $T^{-0.5}$ dependence of the trapping coefficient of the Zn vacancies (giving $\kappa_{V,\mathrm{Zn}}\simeq0.5\lambda_B$ at 30 K). In addition, the escape rate from the Rydberg state of the negative ion has been neglected, since it becomes important only above 50 K. The best estimate for the trapping rate to the O vacancies is obtained from the data at 100–150 K, where the effect of the O vacancies is most visible. Assuming a typical value of $E_b=40$ meV (Ref. 28) for the Rydberg-state binding energy in addition to the $T^{-0.5}$ dependence of the trapping coefficient of the negative-ion-type defect, the (saturated) trapping rate to the O vacancies below 150 K can be estimated as

$$\kappa_{V,\mathrm{O}}=(\lambda_B+\kappa_{\mathrm{st}}^{\mathrm{eff}})\frac{\tau_{\mathrm{ave}}-\tau_B}{\tau_{V,\mathrm{O}}-\tau_{\mathrm{ave}}}-\kappa_{V,\mathrm{Zn}}\frac{\tau_{V,\mathrm{Zn}}-\tau_{\mathrm{ave}}}{\tau_{V,\mathrm{O}}-\tau_{\mathrm{ave}}}\simeq 0.7\lambda_B. \quad (9)$$

The concentrations of the defects can be estimated from the trapping rates in a straightforward matter. Assuming a trapping coefficient of $\mu_{V,\mathrm{Zn}}=3\times10^{15}\mathrm{s}^{-1}$ at 300 K for the Zn vacancy as for the Ga vacancy in GaN,[29] we obtain $[V_{\mathrm{Zn}}]\simeq2\times10^{16}\mathrm{cm}^{-3}$. At 30 K, $\kappa_{\mathrm{st}}\simeq\kappa_{V,\mathrm{Zn}}$, and assuming that the trapping coefficient of the negative-ion-type defect is similar to that of a negative vacancy,[23,26] the concentrations are also similar, $c_{\mathrm{st}}\simeq2\times10^{16}\mathrm{cm}^{-3}$. These results are the same as reported previously.[21] The trapping coefficient of a neutral vacancy is lower than that of a negative vacancy,[30] and taking a value of $\mu_{V,\mathrm{O}}=1\times10^{15}\mathrm{s}^{-1}$ for the neutral O vacancy results in a concentration of $[V_{\mathrm{O}}]\simeq3\times10^{17}\mathrm{cm}^{-3}$. The concentrations of these defects are larger than the impurity concentrations reported by the manufacturer of the samples (Eagle Picher). Hence most of the irradiation-induced point defects are not complexed with the in-grown impurities.

A more detailed picture of the trapping rates to the different defects is obtained by fitting the temperature-dependent trapping model to the τ_{ave} vs T data in Fig. 1. Five fitting parameters are needed in total: three absolute levels of the trapping rates and two parameters to describe the temperature dependence of the trapping to the negative-ion-type defects (Rydberg-state binding energy) and to the O vacancies (binding or ionization energy). Assuming that the temperature dependence of the trapping to the O vacancies is due to the thermal escape of positrons at high temperatures does not fit well to the data, since the changes in the trapping rate are not steep enough to reproduce the experimentally observed temperature-dependent behavior. Hence, we assign the ionization of the neutral O vacancy as the source of the temperature dependence of its trapping rate.

Figure 4 shows the carrier concentration and the position of the Fermi level in the irradiated ZnO samples obtained from temperature-dependent Hall measurements. The O vacancies start to trap positrons effectively below 200 K, where the Fermi level is about $E_C-0.1$ eV. Thus the ionization en-

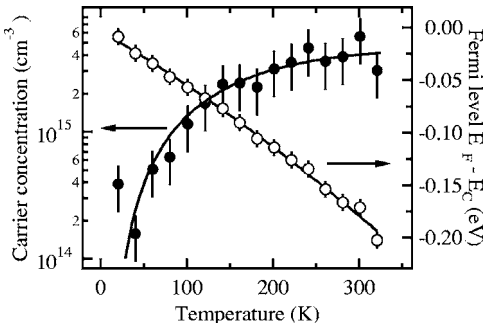

FIG. 4. The carrier concentration measured in irradiated ZnO as a function of temperature. The position of the Fermi energy relative to the conduction-band edge is shown. The solid curves are drawn to guide the eye.

ergy of the O vacancy can be expected to be around 100 meV. Indeed, the fit results in $E_i = 100 \pm 10$ meV.

The fitted trapping rates are shown in the lower panel of Fig. 5. In addition to the ionization energy of the O vacancy, the binding energy to the Rydberg state of the negative-ion-type defect is obtained as $E_b = 40 \pm 10$ meV, similar as observed in GaN.[28] The origin of temperature-dependent behavior of the positron data can be seen from the figure. The trapping rate to the Zn vacancies increases as $T^{-0.5}$ with decreasing temperature, while the thermal detrapping causes the trapping rate to the negative ions to vanish above 150 K. The trapping rates to the two negative defects coincide at temperatures below 70 K.

The trapping rate to the O vacancies is negligible at 300 K, but increases rapidly with decreasing temperature. At temperatures 100–200 K, it is significantly higher than the sum of the trapping rates to the Zn vacancies and the negative-ion-type defects, causing the deviation from the

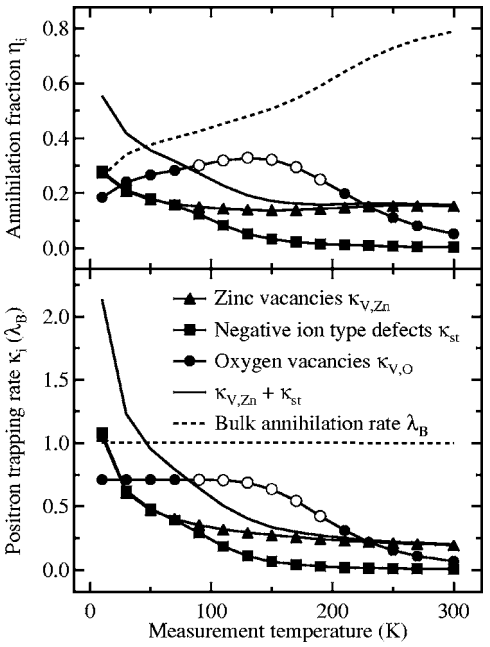

FIG. 5. The positron trapping rates and corresponding annihilation fractions of the different defects as a function of temperature.

one-vacancy-type defect model (straight line) in Fig. 3. Below 100 K, the trapping rate to the negative defects increases very rapidly and the trapping rate to the O vacancies has saturated to a constant value (all the O vacancies are neutral), making the effect of the O vacancies on the positron data small. The effect is seen in the positron annihilation fractions (upper panel of Fig. 5), where it can be observed that the annihilation fraction of the O vacancies exhibits a maximum at around 130 K.

The trapping rates obtained from the fitting are the same as those estimated directly from the data. Thus no revisions are needed to the defect concentrations reported above. The results of the trapping rate fit can be used to obtain an estimate of the Doppler broadening parameters specific to the O vacancy. Fitting the same model to the S vs T and W vs T data with fixed trapping rates and using the O-vacancy-specific S and W parameters as fitting parameters gives $S_{V,O} = 1.003$ (2) and $W_{V,O} = 0.989$ (5). The negative-ion-specific parameters were taken to be those of the bulk—i.e., $S_{st} = W_{st} = S_B = W_B = 1$— and the parameters of the Zn vacancy were fixed at $S_{V,Zn} = 1.039$ and $W_{V,Zn} = 0.87$.[21] The fitted curves are shown in Fig. 3 and in the two upper panels in Fig. 1.

The experimentally obtained annihilation parameters specific to the O vacancy can be compared to those obtained from calculations.[21] The calculations predict that the changes in the parameters (relative to bulk) should be small compared to those of the Zn vacancy, as is observed. The changes are clearly larger than predicted ($\tau^c_{V,O} - \tau^c_B = 3$ ps and $W^c_{V,O} = 0.998$). The calculations in the case of the O vacancy were performed with a theoretically predicted[15] inward relaxation of neighboring atoms of approximately 8%. However in early EPR measurements (at room temperature) on electron-irradiated ZnO the isolated O vacancy has been observed to exhibit a substantial outward relaxation.[11] Performing the same calculations as previously[21] with an outward relaxation of 8% gives a lifetime difference of $\tau^c_{V,O} - \tau^c_B = 20$ ps, in reasonable agreement with the experimental lifetime. The relaxation does not affect significantly the calculated momentum distribution. The theoretical calculations also show that the dominant contribution to the Doppler broadening at high electron momenta (i.e., in the range of the W parameter) comes from the $3d$ electrons of Zn. Hence in the case of the Zn vacancy the W parameter decreases significantly due to the reduced annihilations with the $3d$ electrons of Zn, while in the case of the O vacancy the changes are minimal. The experimental parameters of the O vacancy are practically those of bulk ZnO, which gives further support for the identification of the small open volume defects as the O vacancy rather than a Zn vacancy related complex with a substantial inward relaxation.

The introduction rate of a defect D can be estimated as $\Sigma_D = [D]/\Phi$, where $\Phi = 6 \times 10^{17}$ cm^{-2} is the irradiation fluence. With the defect concentrations $[V_{Zn}] \simeq c_{st} \simeq 2 \times 10^{16}$ cm^{-3} and $[V_O] \simeq 3 \times 10^{17}$ cm^{-3}, the corresponding introduction rates are obtained as $\Sigma_{V,Zn} \simeq \Sigma_{st} \simeq 0.03$ cm^{-1} and $\Sigma_{V,O} \simeq 0.5$ cm^{-1}. The introduction rate of the Zn vacancies is about 30 times lower than determined for Ga vacancies in GaN,[29] manifesting the radiation hardness of ZnO. In addition, as the introduction rates of primary defects are typically

$\simeq 1$ cm^{-1}, both the Zn vacancies and negative ions are probably formed through recombination processes during the irradiation and are thus parts of defect complexes. This is supported by the observations that the isolated Zn vacancies[6] and probably isolated interstitials on both sublattices[12] are mobile well below room temperature. On the other hand, the introduction rate of the O vacancies suggests that *they* are primary defects, and comparison to results obtained from EPR measurements,[11,13] which show that the isolated O vacancy is stable at room temperature, suggests that the O vacancies observed in this work are isolated.

C. Summary

We observe three kinds of point defects produced by the electron irradiation in *n*-type ZnO: vacancies on both sublattices (possibly parts of larger defect complexes) and negative-ion-type defects, attributed to O interstitials or O antisites. The Zn vacancies and the negative ions act as compensating centers, both produced at concentrations $[V_{\mathrm{Zn}}] \simeq c_{\mathrm{st}} \simeq 2\times 10^{16}$ cm^{-3} and are probably parts of larger defect complexes. The irradiation-induced O vacancies are suggested to be isolated and have a deep donor character with the ionization level $E_i = 100 \pm 10$ meV below the conduction band. They are produced at a concentration of $[V_{\mathrm{O}}] \simeq 3 \times 10^{17}$ cm^{-3}. The lifetime of a positron trapped at an O vacancy is determined to be $\tau_{V,\mathrm{O}} = 195 \pm 5$ ps, while it is $\tau_{V,\mathrm{Zn}} = 230 \pm 10$ ps in the Zn vacancy.[21]

IV. THERMAL RECOVERY

A. Positron data

Both the as-grown and irradiated ZnO samples were *in situ* thermally annealed in the positron measurement cryostat for 30 min at temperatures up to 600 K. No changes in the positron parameters were observed in as-grown ZnO. The average positron lifetime measured at four different temperatures in the irradiated samples is presented as a function of annealing temperature in Fig. 6. The positron lifetime decreases with increasing annealing temperature and reaches the level of the as-grown material at the annealing temperature of 590 K, above which no further changes were observed. The two lifetime components $\tau_1 = 150$–180 ps and $\tau_2 = 230 \pm 10$ ps extracted from the data are also shown in Fig. 6 together with the intensity of the second component. The experimental spectra are two-componential up to the highest annealing temperatures, where the separation could be performed only at low measurement temperatures due to the small concentration of the defects.

As can be seen from Fig. 6, the first annealing stage of the irradiation-induced defects occurs at temperatures around 400 K. Figure 7 presents the average positron lifetime as a function of measurement temperature after the annealing steps at 400–430 K. The average positron lifetime decreases by 3–5 ps at all measurement temperatures during this annealing stage. The intensity of the Zn vacancy-related lifetime component $\tau_2 = 230$ ps decreases at this stage (upmost panel in Fig. 6), while the component itself remains constant,

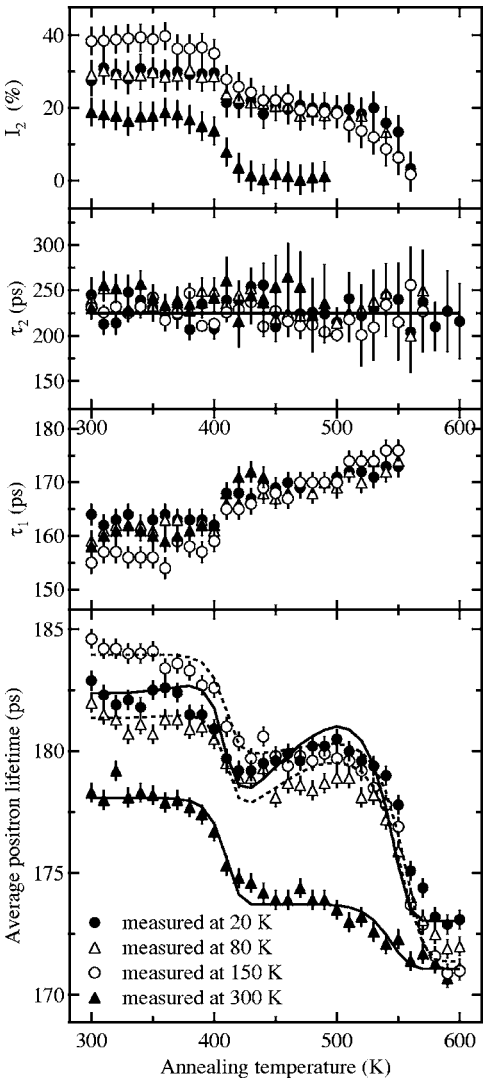

FIG. 6. The average positron lifetime in the irradiated sample as a function of the annealing temperature, measured at 20, 80, 150, and 300 K. The solid curves are obtained from the trapping rate fittings. The two extracted lifetime components are shown in the upper panels together with the intensity of the higher component.

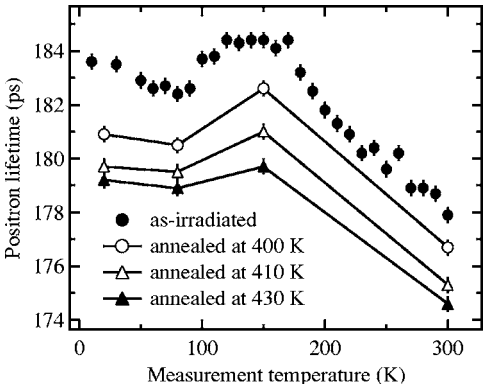

FIG. 7. The average positron lifetime in the irradiated sample annealed at temperatures 400–430 K.

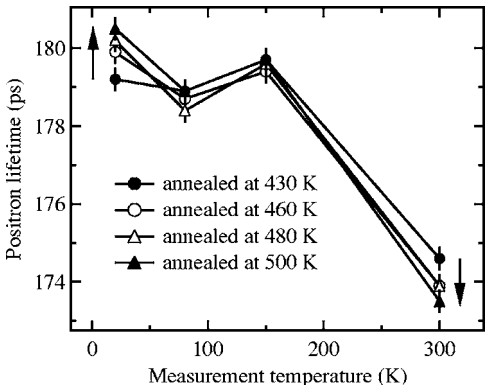

FIG. 8. The average positron lifetime in the irradiated sample annealed at temperatures 430–500 K. The arrows show the direction of increasing annealing temperature.

indicating that part of the Zn vacancies anneal out of the material.

At annealing temperatures 430–500 K the average positron lifetime remains practically constant at measurement temperatures 80 K and 150 K, increases at 20 K, and decreases at 300 K. This causes the τ_{ave} vs T to become steeper (Fig. 8). The increase of the average positron lifetime at low temperatures can be explained by the annealing of the negative-ion-type defects which leads to a larger fraction of positron annihilations at Zn vacancies.

The full recovery of the irradiation-induced defects occurs at annealing temperatures 500–600 K, as can be seen from Figs. 6 and 9. The local maximum in the τ_{ave} vs T plot in Fig. 9 disappears at this last stage, which indicates that O vacancies anneal out simultaneously with the rest of the Zn vacancies. The positron lifetime versus measurement temperature curve in ZnO irradiated and annealed at 600 K is identical to that in as-grown ZnO. This result is in perfect agreement with the results of electrical measurements,[19] where the compensating defects produced by irradiation have been observed to anneal out of the material at around 600 K.

The behavior of the separated lifetime components τ_1 and τ_2 as a function of annealing temperature (Fig. 6) gives further support for the three-defect model presented in Sec. III. The second lifetime component τ_2, specific to the Zn vacancy, remains constant throughout the whole annealing temperature range, implying that it truly represents positrons annihilating in one bound state rather than a superposition of several bound states. The first (lower) lifetime component τ_1 increases abruptly at the first annealing stage, as expected since the trapping rate to the Zn vacancies decreases due to the decrease in their concentration. However, the experimental value of τ_1 after this stage coincides with the bulk lifetime ($\tau_1 = \tau_B = 170$ ps), while it should be lower in the ideal case of positron trapping at Zn vacancies only.[23] In addition, τ_1 increases even above τ_B with further annealing, giving a direct indication that it is mixed with a lifetime component clearly above τ_B. This mixing implies the presence and domination of an additional vacancy defect after the annealing at 500 K, although it is not possible to decompose directly more than two lifetime components due to finite statistics. This vacancy defect is the O vacancy, identified in Sec. III by Doppler broadening measurements.

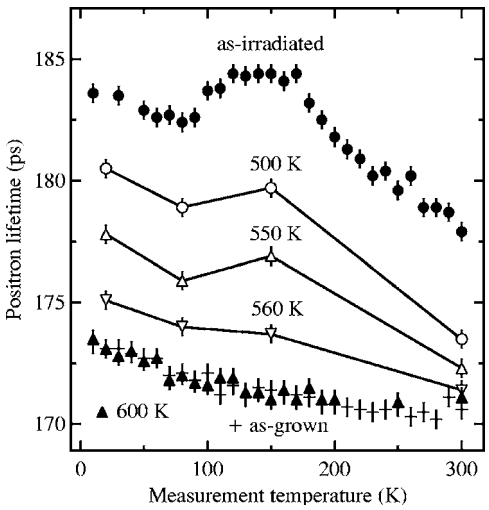

FIG. 9. The average positron lifetime in the irradiated sample annealed at temperatures 500–600 K.

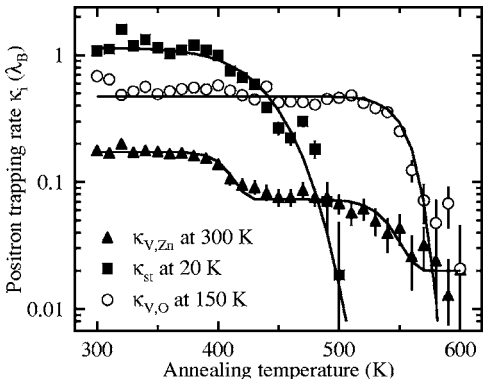

FIG. 10. The positron trapping rates to the different defects as a function of the annealing temperature. The solid curves are fitted to the data.

B. Analysis

It was shown in Sec. III B that the trapping rates to the Zn vacancies, negative-ion-type defects, and O vacancies can be directly estimated from the positron data without fitting. Using Eqs. (7)–(9) the trapping rates to the three defects were calculated as a function of annealing temperature. They are presented in Fig. 10. It is clearly seen that the interpretation of the results presented above is correct: the Zn vacancies anneal out of the material at two separate stages at around 400 K and 550 K, the negative-ion-type defects anneal out around 450 K, and the O vacancies anneal out together with the second part of the Zn vacancies above 550 K. The temperature at which the O vacancies recover is in good agreement with a recent EPR study,[13] where the O vacancies are observed to disappear between 570 K and 670 K.

The activation energies E_A corresponding to the different annealing stages can be fitted to the positron data. Assuming that each defect anneals independently, the isochronal annealing process for a defect concentration N can be described as[19]

$$N_{i+1} = N_\infty + (N_i - N_\infty)\exp[-\nu t \exp(-E_A/kT_i)], \quad (10)$$

where the subscript i denotes the annealing step ($T_i=[300+10\times(i-1)]$ K), $t=1800$ s is the annealing time, and ν is a frequency factor (assumed to be $\nu=10^{13}$ s^{-1}). The trapping rates are directly proportional to the defect concentrations. Thus the trapping rates and activation energies of the annealing stages can be fitted to the data in Fig. 10.

Using the above model, two separate activation energies for the Zn vacancies were fitted, giving $E_{A1}^{V,\mathrm{Zn}}=1.3\pm0.1$ eV and $E_{A2}^{V,\mathrm{Zn}}=1.8\pm0.1$ eV. Here 40% of the irradiation-induced Zn vacancies recover at the first anneling stage. The activation energy of the second stage is in perfect agreement with the value obtained in the electrical measurements for the annealing of the compensating center, $E_A=1.73$ eV.[19] The activation energy of the annealing stage of the O vacancies is fitted as $E_A^{V,\mathrm{O}}=1.8\pm0.1$ eV, which coincides with that of the second stage of the Zn vacancies, as expected.

The recovery of the negative-ion-type defects could not be fitted with a single activation energy. Instead, a linear dependence $E_A^{\mathrm{st}}=E_{A0}^{\mathrm{st}}+\alpha(T_i-T_1)$ was assumed. The fitting gave $E_{A0}^{\mathrm{st}}=1.15$ eV and $\alpha=0.0023$, with the activation energies ranging from 1.4 ± 0.1 eV at the beginning of the anneal at about 400 K to 1.6 ± 0.1 eV at the end at about 500 K. This kind of "sliding" of the activation energy can be expected if the negative-ion-type defects are not all identical and have different diffusion barriers. Another possibility would be that the out-annealing of these defects is not limited only by diffusion, but, e.g., by the transition to the surface or to another lattice site.

The low introduction rate of the Zn vacancies suggests that they have formed complexes with other defects. In addition, already the early EPR studies[6] have shown that the isolated Zn vacancy is mobile well below room temperature. The fact that only the irradiation-induced Zn vacancies have annealed out of the material at 600 K implies that the in-grown Zn vacancies are not isolated (as expected, since they have survived the cooling down from the growth temperatures) and that the complexes formed during the irradiation are different from the in-grown Zn-vacancy-related defect. In addition, the observation of two separate annealing stages of the Zn vacancies indicates that two different defect complexes are formed in the irradiation.

C. Summary

We observe three annealing stages of the point defects produced by electron irradiation in n-type ZnO in the temperature range 300–600 K. The first annealing stage occurs at about 400 K and consists of the recovery of 40% of the irradiation-induced Zn vacancies, with an activation energy of $E_{A1}^{V,\mathrm{Zn}}=1.3\pm0.1$ eV. The second annealing stage covers the temperature range 400–500 K, where the negative-ion-type defects recover, with activation energies ranging from 1.4 ± 0.1 eV at the beginning of the anneal at about 400 K to 1.6 ± 0.1 eV at the end at about 500 K. The third annealing stage occurs at about 550 K and consists of the recovery of the O vacancies and of the remaining irradation-induced Zn vacancies, with an activation energy of $E_{A2}^{V,\mathrm{Zn}}\simeq E_A^{V,\mathrm{O}}=1.8\pm0.1$ eV. The positron data show that the irradiation-induced defects have fully recovered after this final annealing stage, in perfect agreement with the results of electrical measurements.[19]

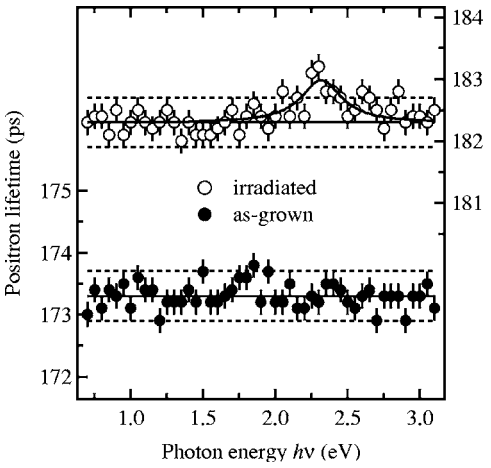

FIG. 11. The average positron lifetime at 20 K in the as-grown and irradiated ZnO samples as a function of illumination photon energy. The solid and dashed lines show the corresponding average lifetimes in the dark ±2 standard deviations. The solid curve is drawn to guide the eye.

V. ILLUMINATION EXPERIMENTS

We studied the optical activity of the in-grown and irradiation-induced defects by shining monochromatic light on the samples during the positron experiments at 20 K. The results are presented in Fig. 11. No effect is observed in the as-grown ZnO samples, where the average positron lifetime remains constant when the photon energy is varied between 0.7 and 3.1 eV. On the other hand, in the irradiated material, a small increase of the average positron lifetime is visible when the photon energy is increased to 2.3 eV, followed by a decrease to the value in the dark with further increase of the photon energy.

Due to limitations imposed by the illumination equipment, the photon flux decreased above 2.4 eV. In order to confirm that the decrease in the average positron lifetime above 2.3 eV is not due this decrease in the photon flux, we performed measurements with different photon fluxes at 2.3 eV. As can be seen from Fig. 12, the average positron lifetime increases up to a photon flux of 7×10^{14} cm^{-2} s^{-1}. The average lifetime stays at the same increased level when the flux is further increased to 6×10^{15} cm^{-2} s^{-1} with the help of 540-nm lasers, which shows that the optically active electrons have reached an equilibrium already at the flux of 7×10^{14} cm^{-2} s^{-1}. Thus the increase of the positron lifetime at photon energy 2.3 eV in Fig. 11 is not limited by the applied photon flux and the behavior of the positron lifetime as a function of illumination photon energy in the irradiated samples is caused by two separate optical processes.

The behavior of the average positron lifetime under illumination at low temperature in Fig. 11 can be explained in the following way. As seen from Fig. 5, the positron data are

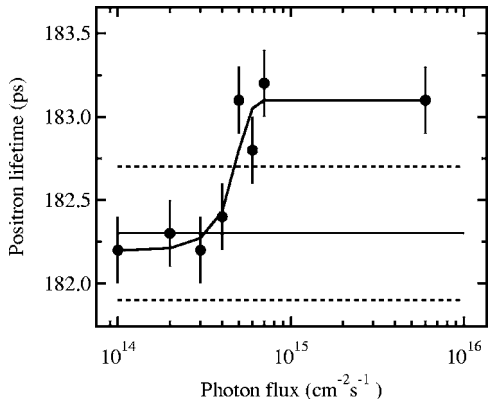

FIG. 12. The average positron lifetime at 20 K in the irradiated ZnO samples as a function of illumination photon ($E=2.3$ eV) flux. The solid and dashed lines show the corresponding average lifetimes in the dark ±2 standard deviations. The solid curve is drawn to guide the eye.

dominated by the Zn vacancies and negative-ion-type defects at the measurement temperature of 20 K. Thus it is natural to assign the observed optical activity to these defects. The Zn vacancies are mostly in the double-negative-charge state[21] (and cannot become more negative), and hence the increase of the average positron lifetime when approaching the illumination photon energy of 2.3 eV from below indicates that the negative-ion-type defects become less negative or even neutral and start trapping positrons less efficiently, increasing the fraction of positron annihilations at the Zn vacancies. The subsequent decrease of the positron lifetime with the further increase of the illumination photon energy then indicates that the Zn vacancies become less negative in their turn. This can be interpreted as both the Zn vacancies and the negative ions having an ionization level close to 2.3 eV. According to theoretical calculations,[15] the $V_{\mathrm{Zn}}^{2-/-}$ transition should occur at $E_C-2.6$ eV, in good agreement with our data. The same work predicts that the O interstitial (octahedral position) has the $O_I^{2-/-}$ transition at $E_C-2.4$ eV and the O antisite has the $O_{\mathrm{Zn}}^{2-/0}$ transition at $E_C-2.3$ eV. This supports the tentative identification of the negative ion as the O_I or O_{Zn}.

All the optical activity is lost after the thermal annealings, and the τ_{ave} versus photon energy of the irradiated samples annealed at 600 K coincides with that of the as-grown samples. The free-electron concentration in both the as-grown and irradiated and annealed ZnO is 30 times larger than after the irradiation. Thus, even if there were an optical transition at around 2.3 eV in the as-grown material, it would probably not be observed with the photon fluxes used in this work since the recombination rate is higher due to free electrons. The electron level at 2.3 eV below the conduction band correlates with the energy of the emitted light in green luminescence.[14] Thus the Zn vacancies, which have the lowest defect formation energy in *n*-type ZnO,[15] could be involved in the transition giving rise to the green luminescence.

VI. CONCLUSIONS

We have applied positron annihilation spectroscopy to study the point defects introduced by 2-MeV electron irradiation at room temperature in *n*-type ZnO. The measurements were performed at 10–300 K. We studied the optical activity of the irradiation-induced defects by shining monochromatic light on the samples during the positron measurements at 20 K. The thermal recovery of the defects produced by the irradiation was studied by 30-min annealings of the samples at 300–600 K.

We observe three kinds of point defects produced by the electron irradiation: vacancies on both sublattices and negative-ion-type defects, tentatively identified as O interstitials. The Zn vacancies and the negative ions act as compensating centers, both produced at concentrations $[V_{\mathrm{Zn}}]\simeq c_{\mathrm{st}}\simeq 2\times 10^{16}$ cm^{-3}. The irradiation-induced O vacancies are deep donors with the ionization level about 100 meV below the conduction band and produced at a concentration of $[V_{\mathrm{O}}]\simeq 3\times 10^{17}$ cm^{-3}. The lifetime of a positron trapped at an O vacancy is determined to be $\tau_{V,\mathrm{O}}=195\pm 5$ ps, while it is $\tau_{V,\mathrm{Zn}}=230\pm 10$ ps in the Zn vacancy.

The irradiation-induced defects fully recover after the annealing at 600 K, in good agreement with electrical measurements. The Zn vacancies anneal out of the material in two stages with fitted activation energies $E_{A1}^{V,\mathrm{Zn}}\simeq 1.3$ eV and $E_{A2}^{V,\mathrm{Zn}}\simeq 1.8$ eV, indicating that the Zn vacancies are parts of two different defect complexes. The O vacancies anneal simultaneously with the Zn vacancies at the later stage with fitted activation energy $E_A^{V,\mathrm{O}}\simeq 1.8$ eV. The negative-ion-type defects anneal out between the two annealing stages of the Zn and O vacancies. No single activation energy could be fitted to this annealing stage, indicating that the recovery of these defects is not limited only by the diffusion in the lattice.

By shining monochromatic light on the samples during the positron annihilation measurements at low temperature, we find that both the irradiation-induced Zn vacancies and the negative-ion-type defects have ionization levels close to 2.3 eV. Based on this we suggest that the negative ions are oxygen interstitials or oxygen antisites in the negative-charge state (similarly to the Zn vacancies). No optical activity was observed in the as-grown ZnO or in the irradiated ZnO after annealing at 600 K. Since the Zn vacancies have the lowest defect formation energy in *n*-type ZnO, it is likely that they are involved in the transition responsible for the green luminescence in ZnO.

ACKNOWLEDGMENTS

We wish to thank G. Cantwell for providing the samples. F.T. acknowledges financial support from Emil Aaltonen and Jenny and Antti Wihuri foundations and from the Research Foundation of Helsinki University of Technology. D.C.L. was supported by U.S. Air Force Contract No. F33615-00-C-5402.

*Electronic address: filip.tuomisto@tkk.fi

[1] D. C. Look, D. C. Reynolds, J. R. Sizelove, R. L. Jones, C. W. Litton, G. Cantwell, and W. C. Harsch, Solid State Commun. **105**, 399 (1998).
[2] K. K. Kim, H. S. Kim, D. K. Hwang, J. H. Lim, and S. J. Park, Appl. Phys. Lett. **83**, 63 (2003).
[3] Y. R. Ryu, T. S. Lee, and H. W. White, Appl. Phys. Lett. **83**, 87 (2003).
[4] D. C. Look, G. M. Renlund, R. H. Burgener II, and J. R. Sizelove, Appl. Phys. Lett. **85**, 5269 (2004).
[5] P. Sharma, A. Gupta, K. V. Rao, F. J. Owens, R. Sharma, R. Ahuja, J. M. Osorio Guillen, B. Johansson, and G. A. Gehring, Nat. Mater. **2**, 673 (2003).
[6] D. Galland and A. Herve, Solid State Commun. **14**, 953 (1974).
[7] D. Galland and A. Herve, Phys. Lett. **33A**, 1 (1970).
[8] K. Leutwein and J. Schneider, Z. Naturforsch. A **26**, 1236 (1971).
[9] A. L. Taylor, G. Filipovich, and G. K. Lindeberg, Solid State Commun. **8**, 1359 (1970).
[10] J. M. Smith and W. E. Vehse, Phys. Lett. **31A**, 147 (1970).
[11] C. Gonzales, D. Galland, and A. Herve, Phys. Status Solidi B **72**, 309 (1975).
[12] Y. V. Gorelkinskii and G. D. Watkins, Phys. Rev. B **69**, 115212 (2004).
[13] L. S. Vlasenko and G. D. Watkins, Phys. Rev. B **71**, 125210 (2005).
[14] D. C. Reynolds, D. C. Look, B. Jogai, and H. Morkoc, Solid State Commun. **101**, 643 (1997).
[15] A. F. Kohan, G. Ceder, D. Morgan, and Chris G. Van de Walle, Phys. Rev. B **61**, 15019 (2000).
[16] K. Vanheusden, C. H. Seager, W. L. Warren, D. R. Tallant, and J. A. Voight, Appl. Phys. Lett. **68**, 403 (1995).
[17] K. Vanheusden, W. L. Warren, C. H. Seager, D. R. Tallant, J. A. Voight, and B. E. Gnade, J. Appl. Phys. **79**, 7983 (1996).
[18] H.-J. Egelhaaf and D. Oelkrug, J. Cryst. Growth **161**, 190 (1996).
[19] D. C. Look, D. C. Reynolds, J. W. Hemsky, R. L. Jones, and J. R. Sizelove, Appl. Phys. Lett. **75**, 811 (1999).
[20] A. Y. Polyakov *et al.*, J. Appl. Phys. **94**, 2895 (2003).
[21] F. Tuomisto, V. Ranki, K. Saarinen, and D. C. Look, Phys. Rev. Lett. **91**, 205502 (2003).
[22] C. Coskun, D. C. Look, G. C. Farlow, and J. R. Sizelove, Semicond. Sci. Technol. **19**, 752 (2004).
[23] K. Saarinen, P. Hautojärvi, and C. Corbel, in *Identification of Defects in Semiconductors*, edited by M. Stavola (Academic Press, New York, 1998), p. 209.
[24] K. Saarinen, A. P. Seitsonen, P. Hautojärvi, and C. Corbel, Phys. Rev. B **52**, 10932 (1995).
[25] C. Corbel, F. Pierre, K. Saarinen, P. Hautojärvi, and P. Moser, Phys. Rev. B **45**, 3386 (1992).
[26] M. J. Puska, C. Corbel, and R. M. Nieminen, Phys. Rev. B **41**, 9980 (1990).
[27] J. Oila, J. Kivioja, V. Ranki, K. Saarinen, D. C. Look, R. J. Molnar, S. S. Park, S. K. Lee, and J. Y. Han, Appl. Phys. Lett. **82**, 3433 (2003).
[28] K. Saarinen, J. Nissilä, P. Hautojärvi, J. Likonen, T. Suski, I. Grzegory, B. Lucznik, and S. Porowski, Appl. Phys. Lett. **75**, 2441 (1999).
[29] K. Saarinen, T. Suski, I. Grzegory, and D. C. Look, Phys. Rev. B **64**, 233201 (2001).
[30] J. Mäkinen, C. Corbel, P. Hautojärvi, P. Moser, and F. Pierre, Phys. Rev. B **39**, 10162 (1989).